ANNALS OF GEOPHYSICS, 69, 2, SA216, 2026, doi:10.4401/ag-9465
OPEN ACCESS

Study of the F-region topside in situ ionospheric density using COSMIC-2/ICON satellite observations and comparison with the IRI-2020 model predictions

Awuor Adero[*,1], Solomon Otoo Lomotey[2], Hellen Babirekere[3], Vladimir Truhlik[4], Daniel Okoh[1,5], Ola Abu Elezz[6], John Bosco Habarulema[7], Ebenezer Agyei-Yeboah[8], Paul Baki[1], George Ochieng[1], Geovian Stower[9]

(1) Technical University of Kenya, Department of Physics, Earth and Environmental Sciences, Nairobi, Kenya
(2) University of Environment and Sustainable Development (UESD), Department of Physical and Mathematical Sciences, Somanya, Ghana
(3) Busitema University, Department of Physics, Uganda
(4) Institute of Atmospheric Physics of the Czech Academy of Sciences, Department of Ionosphere and Aeronomy, Prague, Czech Republic
(5) National Space Research and Development Agency (NASRDA), Abuja, Nigeria
(6) Space Weather Monitoring Center, Capital University, Egypt
(7) South African National Space Agency (SANSA), Hermanus, South Africa
(8) Laboratorio de Física e Astronomia Universidade do Vale do Paraiba (UNIVAP) Urbanova Sao Jose Dos Campos SP Brazil
(9) Kenya Space Agency, Nairobi, Kenya

Article history: received October 24, 2025; accepted April 16, 2026

Abstract

This study presents a climatological evaluation of the International Reference Ionosphere (IRI-2020) model predictions of low-latitude topside F-region O^+ and H^+ ion compositions, with particular emphasis on their fractional abundances. In situ O^+ and H^+ measurements from the Ion Velocity Meters (IVM) instruments from the Ionospheric Connection Explorer (ICON) (2020-2022) and Constellation Observing System for Meteorology, Ionosphere and Climate (COSMIC-2) (2021-2023) satellites missions were used as independent observational benchmarks. The IRI-2020 model is sampled along the satellite trajectories at corresponding times, locations, and altitudes to ensure consistent climatological comparisons. Both satellite results revealed pronounced diurnal, seasonal, latitudinal, and longitudinal variability in topside ion fractions. IRI-2020 successfully predicted the large-scale climatological structure of the observed ion composition but exhibits reduced hemispheric asymmetries and smoother day-night transitions relative to the measurements. ICON results showed systematic overestimation of O^+ (approximately 21-37%) and underestimation of H^+ (approximately 12-23%), particularly during equinoxes and around dawn and dusk. In contrast, COSMIC-2-based comparisons show smaller biases for both species. The differences in results, observed from both satellites, likely reflect different conditions of solar activity during the two missions. These results demonstrate that while IRI-2020 provides a robust large-scale global description of topside ion composition, some limitations persist, highlighting the need for improved representation of temporal and spatial resolution and better description of ion composition variation with geophysical parameters.

Keywords: International Reference Ionosphere (IRI-2020); Topside ionosphere; O^+/H^+ fractions; ICON /COSMIC-2 mission

1. Introduction

The ionosphere plays a critical role in near-Earth space by affecting the propagation of radio waves and coupling the neutral atmosphere with the magnetosphere (Mainul and Jakowski, 2012; Ram et al., 2010). Accurate representation of ionospheric plasma density and composition is therefore essential for both scientific investigations and practical applications, including satellite communication, navigation, and space weather forecasting. In the low-latitude topside ionosphere, the relative abundances of dominant ion species, primarily O^+ and H^+, are controlled by a complex interplay of photoionization, chemical recombination, electrodynamic transport, and neutral atmosphere dynamics. These processes exhibit strong variability with local time, season, latitude, longitude, and solar and geomagnetic activity, making reliable empirical modeling especially challenging.

The International Reference Ionosphere (IRI) is the internationally recognized empirical standard for specifying ionospheric plasma parameters from the D region to the topside ionosphere (Bilitza et al., 2017, 2022). Concretely the IRI model provides global, monthly, and diurnal averages or medians of ionospheric parameters such as electron density (Ne), ion temperature (Ti), electron temperature (Te), ion composition (percentages of O^+, H^+, He^+, N^+ etc.), vertical plasma drifts, and the probability occurrence of some of the ionospheric layers. Thus, IRI is widely used in both operational and research contexts due to its comprehensive data coverage and climatological robustness. Recent versions of the model, including IRI-2020, incorporate updated topside electron density formulations and ion composition representations derived from satellite observations and theoretical considerations (Bilitza et al., 2022; Pignalberi et al., 2025). Before these improvements several important studies have demonstrated that uncertainties persist in the representation of topside electron density and ion composition, particularly during low solar activity when the altitude of the transition region where O^+ and H^+ fractions become comparable is very low (e.g., Lühr and Xiong, 2010; Kotov et al., 2015).

Low-latitude topside ion composition is especially sensitive to vertical plasma drifts driven by $\mathbf{E} \times \mathbf{B}$ electrodynamics, thermospheric winds, and the prereversal enhancement (PRE) of the zonal electric field in the evening sector (Fejer et al., 1981, 1991, 2008). These processes can rapidly modify the altitude of the O^+/H^+ transition height, leading to strong local-time and seasonal variability in ion fractions. Because IRI-2020 is fundamentally a monthly-mean climatological model, its ability to reproduce such sharp gradients and transition-region dynamics remains an open question, particularly under low-latitude conditions where electrodynamic forcing is significant.

Recent satellite missions have provided unprecedented opportunities to evaluate empirical ionospheric models using in situ observations. The ICON mission measures ion composition and ion dynamics in the low-latitude topside ionosphere at altitudes ranging from approximately 575 to 600 km (Heelis et al., 2017; Immel et al., 2018). In contrast, the COSMIC-2 (Anthes and Schreiner, 2019) after reaching its final orbital altitude provides extensive low-latitude coverage (6 satellites) at slightly lower altitude (about 530 km).

Recent studies have evaluated the performance of IRI-2020 using either ICON or COSMIC-2 observations. For example, Han et al., (2025) examined IRI-2020 ion temperature models in IRI. Cherniak et al., (2021) assessed the accuracy of COSMIC-2 GNSS radio occultation data for deriving F2 peak parameters and stressed discrepancies with IRI predictions under low solar flux conditions. Hazarika et al., (2024) assessed IRI-2020 performance using COSMIC-2 observations, reporting off-equatorial maxima in the electron density from the IRI model, which are not observed by COSMIC-2.

Regarding ion composition, using incoherent scatter radar (ISR) observations over Arecibo, Vaishnav et al., (2021) investigated the upper transition height, revealing that during low and moderate solar activity conditions, the TBT15 model (Truhlik et al., 2015) overestimates about 5-10% at night and 15-20% in the afternoon but the newer TBT15 model option is more appropriate to investigate variations as compared to the DY85 model (Danilov and Yaichnikov, 1985) option.

While the mentioned studies provide valuable validation, they are largely limited to single-mission or single-station. The recent availability of ion composition observations from the ICON and COSMIC-2 missions, makes it timely to re-evaluate the performance of the IRI-2020 ion composition model. To date, only a small number of studies have examined IRI ion composition in detail, most notably the already mentioned work of Vaishnav et al. (2021), which was based on earlier datasets. Moreover, ICON and COSMIC-2 observations have not previously been used together for a systematic validation of IRI-2020 O^+ and H^+ fractions in the low-latitude topside ionosphere.

In this study, we provide the first climatological evaluation of IRI-2020 topside ion composition using complementary in situ measurements from both ICON and COSMIC-2 Ion Velocity Meters. The two satellite missions sample different altitude ranges and solar activity conditions, allowing us to assess the robustness of

the IRI-2020 TBT15 ion composition model, which is based primarily on older datasets from previous solar cycles. By comparing O^+ and H^+ fractions under different local-time, seasonal, altitude, and solar-activity conditions, this work extends recent ICON-COSMIC-2 intercomparison studies that have focused on different parameters than ion composition. Our results provide new insight into the strengths and limitations of the IRI-2020 ion composition model and highlight the need for continued validation as new observations become available during the current solar cycle.

2. Instruments and Data Processing Methods

2.1 Satellite Observations

In this study, data from in situ ion composition measurements were obtained from IVM-ICON and the COSMIC-2 (also known as FORMOSAT-7) satellite missions. ICON satellite was launched in October 2019 into a low-inclination (~27°), circular orbit at an altitude of approximately 575-600 km, providing dense sampling of the low-latitude topside ionosphere (Immel et al., 2018). The IVM instrument measures ion drift velocities and fractional ion composition, including O^+ and H^+, with high temporal resolution along the satellite trajectory. The fractional ion composition is measured using Retarding Potential Analyzer (RPA) method. In this study, ICON observations spanning January 2020 to December 2022 were analyzed.

The COSMIC-2 constellation consists of six satellites launched in June 2019 into low-inclination orbits (~24°). They reached their designated mission orbits in February 2021 which were almost circular with altitudes ranging from approximately 510 to 550 km. COSMIC-2 provides extensive low-latitude coverage and samples slightly lower altitude range than ICON. Ion composition data from COSMIC-2 covering March 2022 to December 2023 were used in this analysis. The method used to measure ion composition was the same as for ICON, i.e., using RPA, but with higher time resolution (named as "rapid data"). Together, the two datasets offer complementary perspectives on topside ion composition often near the upper transition height.

2.2 Ion Composition Data Model in IRI-2020

IRI-2020 model was used to generate ion composition predictions corresponding to the satellite observations. The model was executed using the IRI-2020 TBT15 topside ion composition option, which provides ion fractions based on empirical formulation employing spherical harmonics fitted to satellite observations (i.e., ion composition resulting from ion mass spectrometer measurements) in invdip vs. magnetic local time coordinates (Truhlik et al., 2015; Bilitza et al., 2022). TBT15 option is an improved version of the model developed by Třísková et al., (2003). Geophysical and solar background conditions were specified internally by IRI-2020 using actual files with indices.

2.3 Data Processing and Model-Data Sampling

The O^+ and H^+ ion fractions were obtained directly from the measured ion composition observations from ICON and COSMIC-2 satellites. All measurements were subjected to quality checks before analysis and measurements (e.g., ion fractions $\geq$1 were discarded as nonphysical values). All observations include basic parameters as Universal Time (UT), geographic coordinates and altitude. From this, calendar date, day of year, solar local time (LT), and magnetic latitude (MLT) were calculated. To construct climatological distributions suitable for comparison with the empirical IRI-2020 predicted values, the satellite observations were first binned into 10-s UT intervals along the satellite orbits (Han et al., 2025) and for each interval and the same geographic coordinates and altitude the IRI model was calculated.

The 10-second data averages obtained from satellites and IRI were further processed using averaging in two-dimensional bins a) local time vs. magnetic latitude and b) geographic longitude vs. magnetic latitude. In the first case we used 1-hour local time intervals from 0 to 24 h and 5° magnetic latitude intervals covering $\pm$40°. In the second case the geographic longitude was binned into 10° intervals spanning $\pm$180°, and magnetic latitude was binned into 5° intervals. For the seasonal analysis, the satellite and modeled ion fractional composition datasets were organized into four seasons using $\pm$15-day temporal windows centered on the equinoxes (20 March and

23 September) and solstices (21 June and 21 December). We additionally used statistical metrics such as correlation and percentage error or bias to quantify the model performance.

3. Results

3.1 ICON satellite observations Vs IRI-2020 model predictions

This section compares ICON satellite O^+ and H^+ ion fraction observations with corresponding IRI-2020 predictions. The analysis is organized into climatological seasons: Vernal Equinox, Autumnal Equinox, December Solstice, and June Solstice.

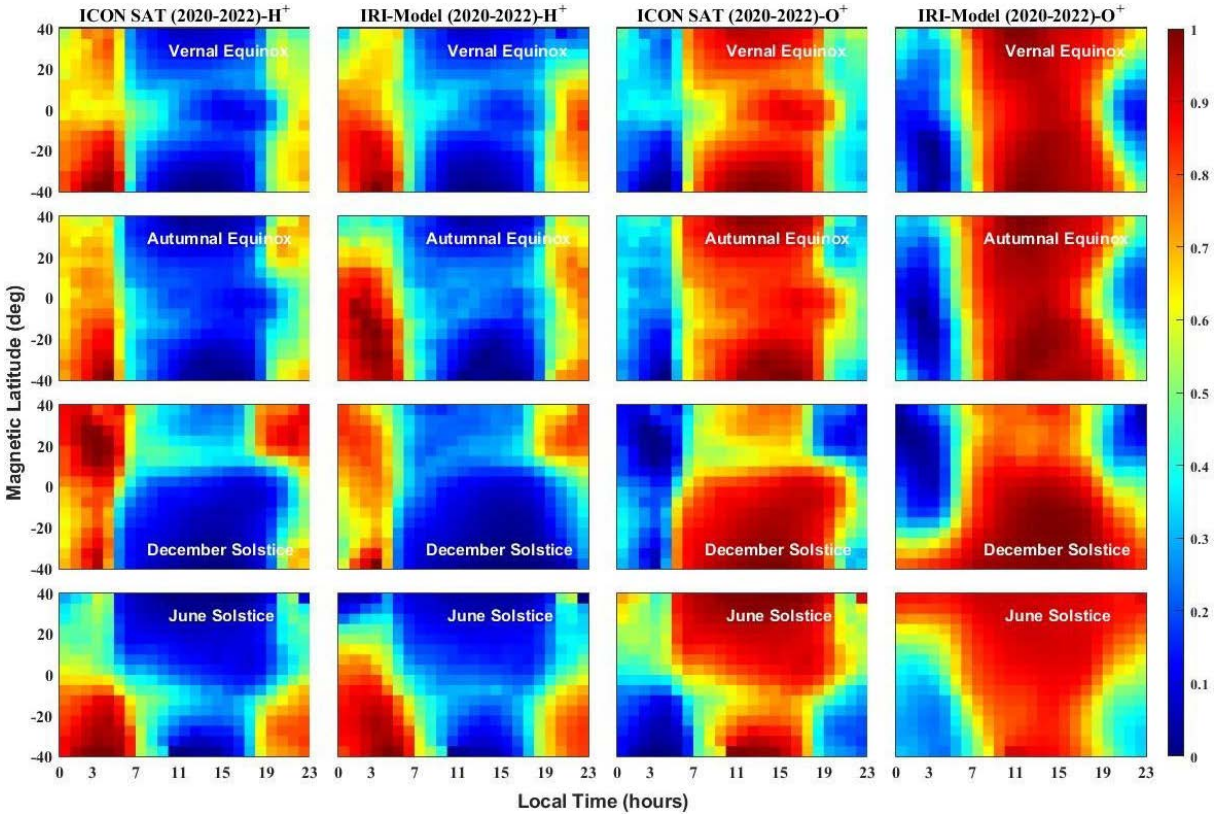

Figure 1. Contour plot displays H^+ and O^+ fractions variation as a function of local time and magnetic latitude (left y-axis), as obtained by the ICON satellite and its corresponding IRI-2020 model predictions (2020-2022).

Figure 1 presents seasonal contour maps of topside H^+ and O^+ ion fractions as a function of LT (0-23 LT) and magnetic latitude, comparing ICON observations with IRI-2020 predictions. During vernal equinox, ICON observed H^+ exhibits enhancement at low to mid-latitudes during nighttime hours. The model reproduces the broad structure but in majority of bins underestimates H^+. The corresponding O^+ panel shows reduced nighttime fractions which then peak during daytime at latitudes around ± 40 degrees. IRI-2020 model shows overestimation of O^+ especially during daytime. In autumnal equinox, ICON observations indicate a weaker latitudinal gradient in H^+ compared to the vernal equinox. The model captures the day-night transition but smooths the latitudinal structure. For the December solstice, H^+ fractions obtained from ICON increase strongly in the Northern Hemisphere (NH), especially during nighttime. IRI-2020 underestimates H^+ at mid-latitudes and near the equator. O^+ fractions also show strong hemispheric asymmetry in both the data and the model, but it is slightly weaker in the model. Finally, during June solstice the ICON reveals enhanced H^+ in the Southern Hemisphere (SH) and reduced values in NH. IRI-2020 reproduces the seasonal trend but shifts the maxima in latitude and local time. O^+ fractions are overestimated by IRI-2020 during nighttime but underestimated during daytime. Throughout all seasons, the measured values from

ICON show somewhat different structures and gradients depending on latitude and LT as compared to the model, which tends to smooth out both ion fractions.

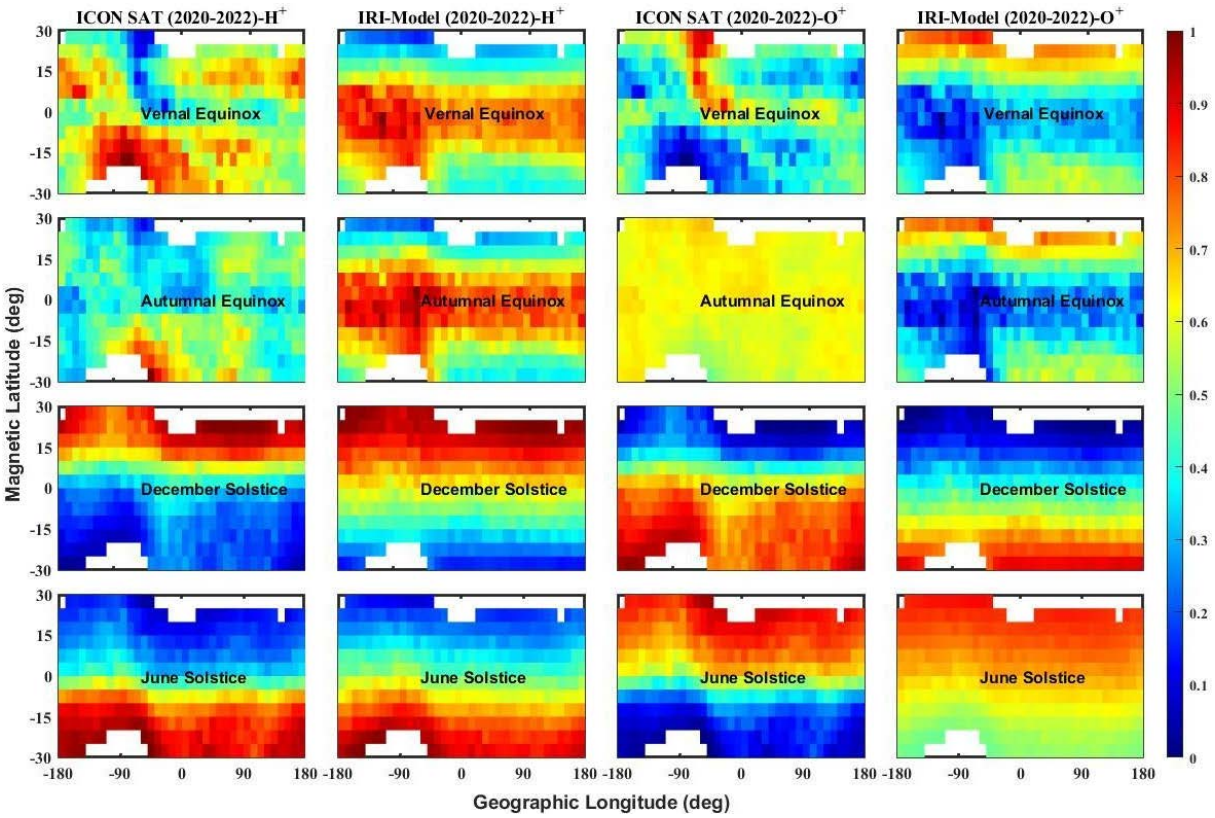

Figure 2. Contour plot displays seasonal variation fractions of H^+ and O^+ as a function of geographic longitude and magnetic latitude (left y-axis), as observed by the ICON satellite and their corresponding IRI-2020 model predictions (2020-2022).

Figure 2 shows the seasonal distributions of H^+ and O^+ fractional compositions as functions of geographic longitude and magnetic latitude, derived from ICON observations and corresponding IRI-2020 predictions for 2020-2022. During the vernal equinox, ICON observations show rather complicated pattern with an enhancement of the O^+ fraction at a longitude of –90 degrees in NH. H^+ fractions show an inverse pattern. In the autumnal equinox, ICON observation again reveals not very clear pattern and while in the case of the H^+ fraction it shows a noticeable longitudinal dependence, for the O^+ fraction rather uniform shape is seen. IRI-2020 shows similar shape for both equinoxes with maximum H^+ fraction at equatorial and low latitudes. Conversely, H^+ from the model shows an "inverse" shape.

During December solstice, ICON measurement shows enhanced O^+ fractions in SH and increased H^+ fractions in NH. Clear latitudinal asymmetries are present. The model, however, reproduces the hemispheric differences but weakens the longitudinal dependence. Similar hemispheric asymmetry is observed in June solstice with elevated O^+ fractions in the NH and enhanced H^+ fractions in the SH. IRI-2020 captures the broad structure but underrepresents localized structures and their maxima.

Figure 3, in general, shows suppressed (stronger) daytime (nighttime) H^+ fractions, panels (a1-d1) and the reverse for the case of O^+ fractions, panels (e1-h1). For H^+ fractions ICON satellite shows a clear diurnal cycle, with minima towards afternoon hours and maxima during the night shifted close to the dawn sector. IRI-2020 reproduces the overall diurnal shape but with comparatively reduced amplitude. The total seasonal error is calculated for each season and shown in panels a2-d2 and e2-h2, alongside the pointwise difference between IRI-2020 predictions and satellite observations curve. The calculated percentage error represents the seasonal magnitude of deviation between the satellite observations and the IRI-2020 predictions, normalized by the total satellite observed ion fractions. The error panels (a2-d2) show predominantly negative percentage values, with peak deviations occurring

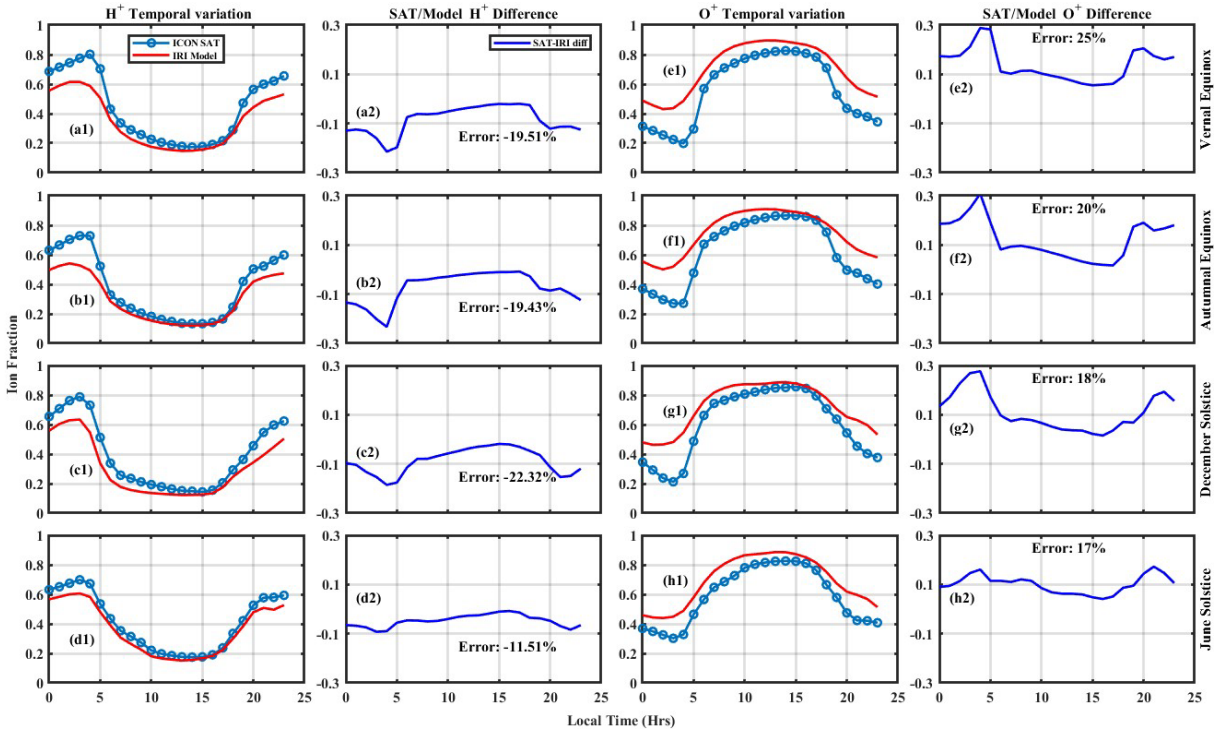

Figure 3. Climatological local-time (0-23 LT) variation of topside H^+ and O^+ ion fractions observed by ICON (blue dotted curves) and predicted by IRI-2020 (red curves), together with the percentage error (seasonal magnitude of deviation) for each season. Panels a1-d1 and e1-h1 show the satellite-model comparison, while panels a2-d2 and e2-h2 display pointwise difference between IRI-2020 predictions and satellite observations and the associated percentage error.

near dawn. Clearly, the model is underestimating the H^+ fractions, in all the seasons. The model poorly performs before sunrise and post-sunset hours, when disparities are most noticeable. Seasonally, the underestimation is greatest during the December solstice (% error: −22.32) and lowest during the June solstice (% error: −11.51). Both the equinoxes recorded nearly the same percentage error values (−19%). O^+ (e1-h1), also exhibits the error predominant before sunrise and post-sunset hours. The modeled results, on the other hand, consistently shows an overestimation around the same local times (dawn and dusk sectors). Both the satellite and model depict the diurnal behaviour of O^+ (Fig. 3, e1-h1), with values increasing after sunrise, peaking about 12-16 LT (~0.8), and decreasing after sunset. 25% (vernal equinox), 20% (autumnal equinox), 18% (December solstice), and 17% (June solstice) are the percentage IRI-SAT discrepancies.

Figure 4 shows that both ICON and IRI-2020 depict a clear latitudinal structure, with H^+ fractions, panels (a1-d1), being underestimated while the O^+ fractions, panels (e1-h1) being overestimated. The model also performs quite well around the equator, $\pm 10°$, for both ion fractions. Furthermore, during solstice seasons, both ion fractions exhibit sharp gradients near the equator, compared to equinoxes, where the gradients are nearly flat. During the equinox, the H^+ (a1-b1) fractions show a different variation with latitude than IRI-2020, which, contrary to observations, does not show a local minimum at the equator. This is opposite in O^+ fractions (e1-f1). During December solstice, satellite observations show clear hemispheric asymmetry, with higher H^+ fractions in SH (panel c1) and enhanced O^+ fractions in NH (panel g1). Strongest hemispheric contrast is exhibited during June solstice. The satellite records elevated H^+ fractions in NH and reduced values in SH, panel d1. IRI-2020 reproduces the sign of this asymmetry but underestimates its amplitude (percentage error ranges between −12 and −22%). O^+ fractions (panel h1), on the other hand, depicts the exact opposite trend, with the model overestimating in this case (percentage error ranges between 17-25%).

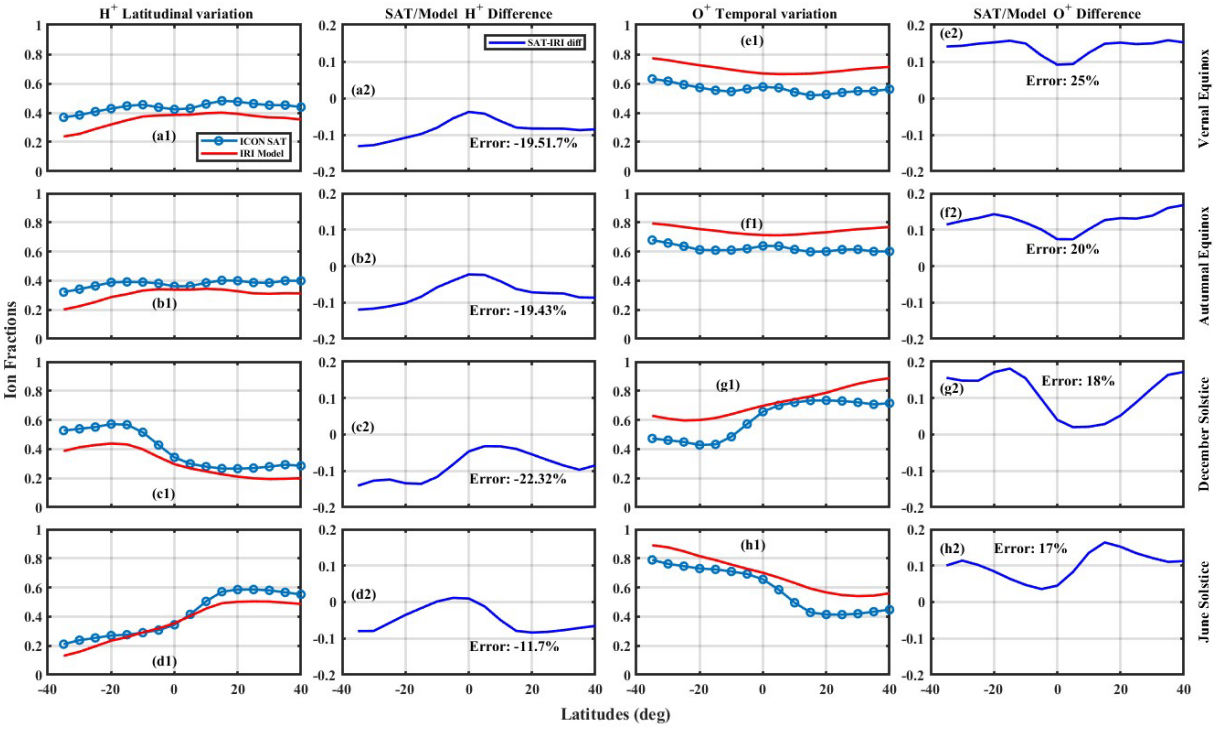

Figure 4. Latitudinal distribution of mean H^+ and O^+ ion fractions derived from ICON observations (blue dotted curves) and corresponding IRI-2020 predictions (red curves), together with the percentage error (seasonal magnitude of deviation) for eac h season. Panels a1-d1 and e1-h1 show the satellite-model comparison, while panels a2-d2 and e2-h2 display pointwise difference between IRI-2020 predictions and satellite observations and the associated percentage error.

3.2 COSMIC-2 satellite observations vs. IRI-2020 model predictions

This section briefly describes and compares the results obtained from COSMIC-2 satellite and IRI-2020 model predictions.

Figure 5 shows seasonal climatological contour plots of H^+ and O^+ fractions as functions of LT and magnetic latitude from COSMIC-2 observations and corresponding IRI-2020 predictions. During vernal equinox, COSMIC-2 H^+ fractions show clear nocturnal enhancement at low and mid-latitudes, with maxima before dawn. The IRI-2020 reproduces the broad structure but misrepresents details in latitudinal variation. O^+ fractions, on the other hand, peak during daytime and decreasing at night. IRI-2020 captures the daytime dominance of O^+ but some underestimation is evident in the post-noon and the post-sunset sectors. The autumnal equinox is very similar to the vernal equinox as shown by both the data and the model. For the December solstice, strong hemispheric asymmetry is evident. COSMIC-2 shows enhanced H^+ in NH. IRI-2020 captures the asymmetry but overestimates its amplitude. In the June solstice, similar patterns persist with the reversal of the hemispheres.

Figure 6 shows longitude-latitude seasonal distributions of H^+ and O^+ fractions from COSMIC-2 and corresponding IRI-2020 predictions from 2022-2023 according to seasons. During Vernal equinox, satellite observed H^+ fractions weaken near the magnetic equator and increase towards higher magnetic latitudes while O^+ fractions show the reverse trend. The IRI-2020 model reproduces the broad equatorial structure but smooths longitudinal gradients, with both ion fractions peaking near magnetic equator. In Autumnal equinox enhanced longitudinal modulation is observed by COSMIC-2, especially for H^+. O^+ fractions show sharper equatorial confinement. The model, on the other hand, shows weaker longitudinal variation. The model overestimates H^+ and underestimates of O^+ near the equator. The December solstice panels reveal clear hemispheric asymmetry. H^+ fractions increase in NH while O^+ fractions decreases and the reverse is observed in SH. The model, however, shows different values with H^+ being overestimated and O^+ underestimated. In June solstice, COSMIC-2 shows enhanced H^+ and O^+ fractions in the SH

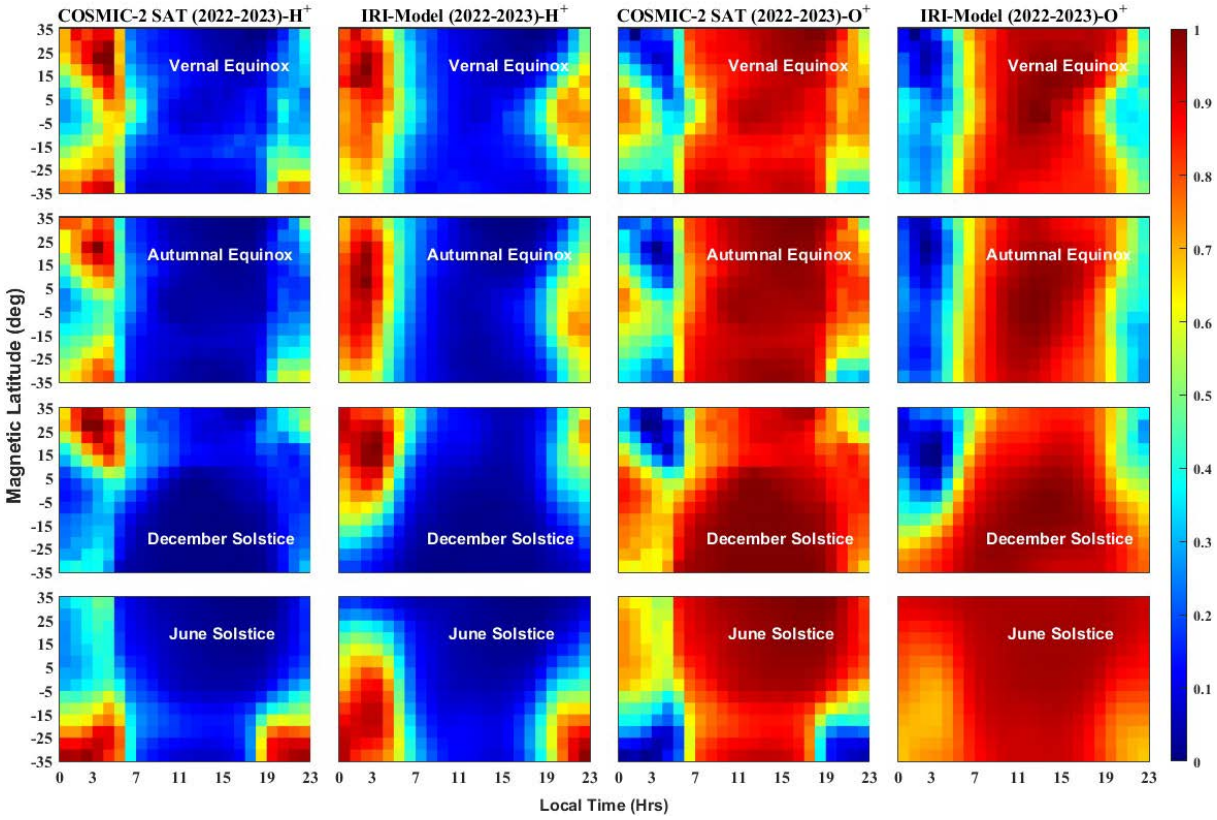

Figure 5. Same as Fig. 1, but for COSMIC-2.

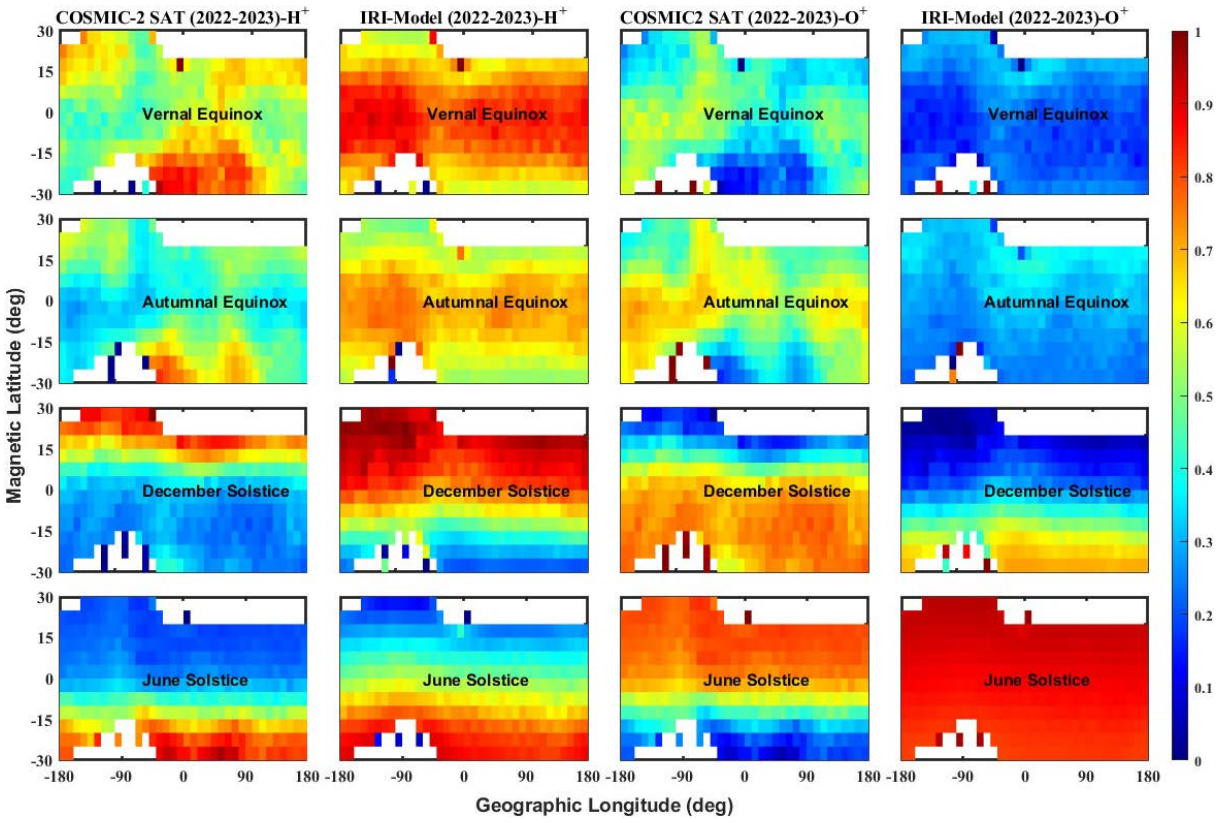

Figure 6. Same as Fig. 2 but for COSMIC-2.

and NH respectively. The IRI-2020 model reveals smoother distributions, with O^+ fractions being overestimated in both hemispheres. In June solstice the model shows almost no hemispheric contrast.

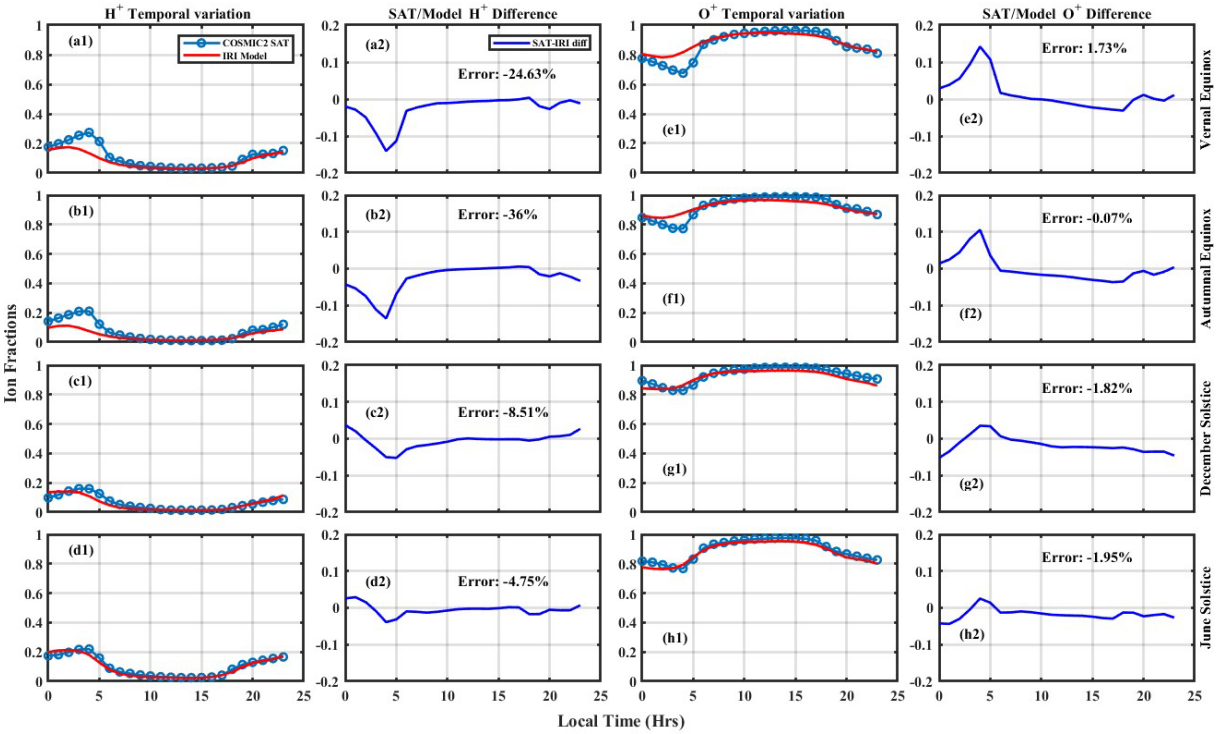

Figure 7. Same as Fig. 3 but for COSMIC-2 satellite.

Similarly to ICON satellite observations (Fig. 3), COSMIC-2 satellite (Fig. 7) also records a suppressed (stronger) daytime (nighttime) H^+ fractions, panels (a1-d1) and opposite for the case of O^+ fractions, panels (e1-h1). However, with smaller error margins compared to ICON satellite measurement. For H^+ fractions, panels (a1-d1), the model agrees relatively well with the data, but tends to underestimate the pre-dawn sector during the equinox in particular, when struggling with relatively rapid changes in local time. The recorded large percentage errors during equinoxes (−36%, autumnal and −24.6%, vernal) are predominantly from the pre-dawn sector, 01-04 LT. The error reduces during the solstice seasons, with the percentage discrepancies of: −4.75% and −8.5% for June and December solstices, respectively. The IRI-2020 model performs much better for O^+ fractions (e1-h1), with the percentage error below ±2% in all seasons, panels (e2-h2). However, the model consistently performs poorly (overestimates) during equinoxes, in the pre-dawn sector.

Figure 8 displays Pearson correlation coefficients computed as a function of latitude to quantify agreement between satellite observations and IRI-2020 predictions. The correlations were calculated using the entire diurnal variation at each latitude, to help in assessing the model's ability to reproduce local-time structure in ion fractional composition. Vernal and Autumnal equinoxes were joined. Panels (a) and (b) show the ICON vs. IRI-2020 correlations for O^+ and H^+, respectively. Panels (c) and (d) show the corresponding COSMIC-2 vs. IRI-2020 correlations. In panel (a), the ICON vs. IRI-2020 correlation for O^+ is generally high across low and mid-latitudes. Correlation weakens near the magnetic equator (during equinox) and at higher latitudes, especially in SH and June solstice. The lowest value occurs during equinox, where the correlation coefficient (r) is above 0.85. In panel (b), the ICON vs. IRI-2020 correlation for H^+ remains consistently strong in most latitudes and in all seasons. The correlation generally is similar to that of O^+, with the lowest value of r ~0.85.

In panel (c), COSMIC-2 vs. IRI-2020 correlations for O^+ show similar latitudinal structure but are slightly stronger off the equator than ICON vs. IRI-2020 results. Reduced correlation appears near the dip equator and especially during December solstice ($r = 0.69$) and equinox ($r = 0.78$). In panel (d), COSMIC-2 vs. IRI-2020, H^+ correlation reveals a similar trend. The correlation reduces at the equator, with the lowest $r = 0.64$, recorded during December solstice. During the equinox, the correlation slightly improves but records its lowest r value of 0.73, at about 6°.

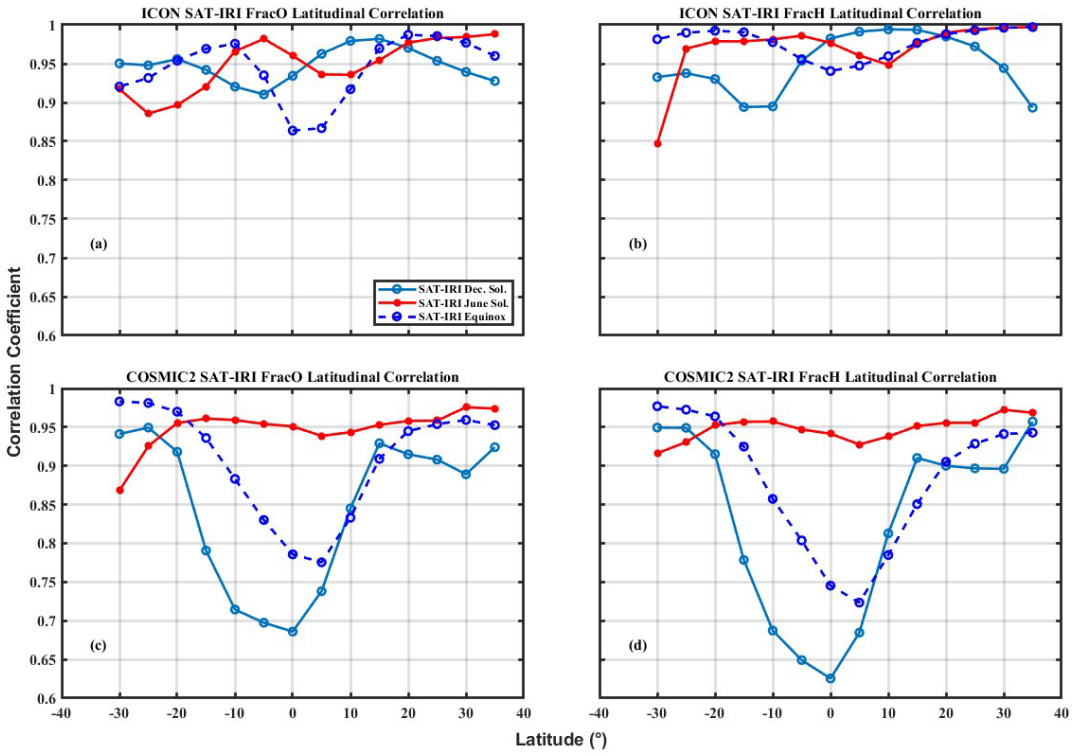

Figure 8. Latitudinal variation of correlation coefficients between the satellite observations and IRI predictions of O^+ and H^+, during various seasons. Panels (a) and (b) show the ICON vs. IRI-2020 O^+ and H^+ correlations respectively while panels (c) and (d) present COSMIC-2 vs. IRI correlations.

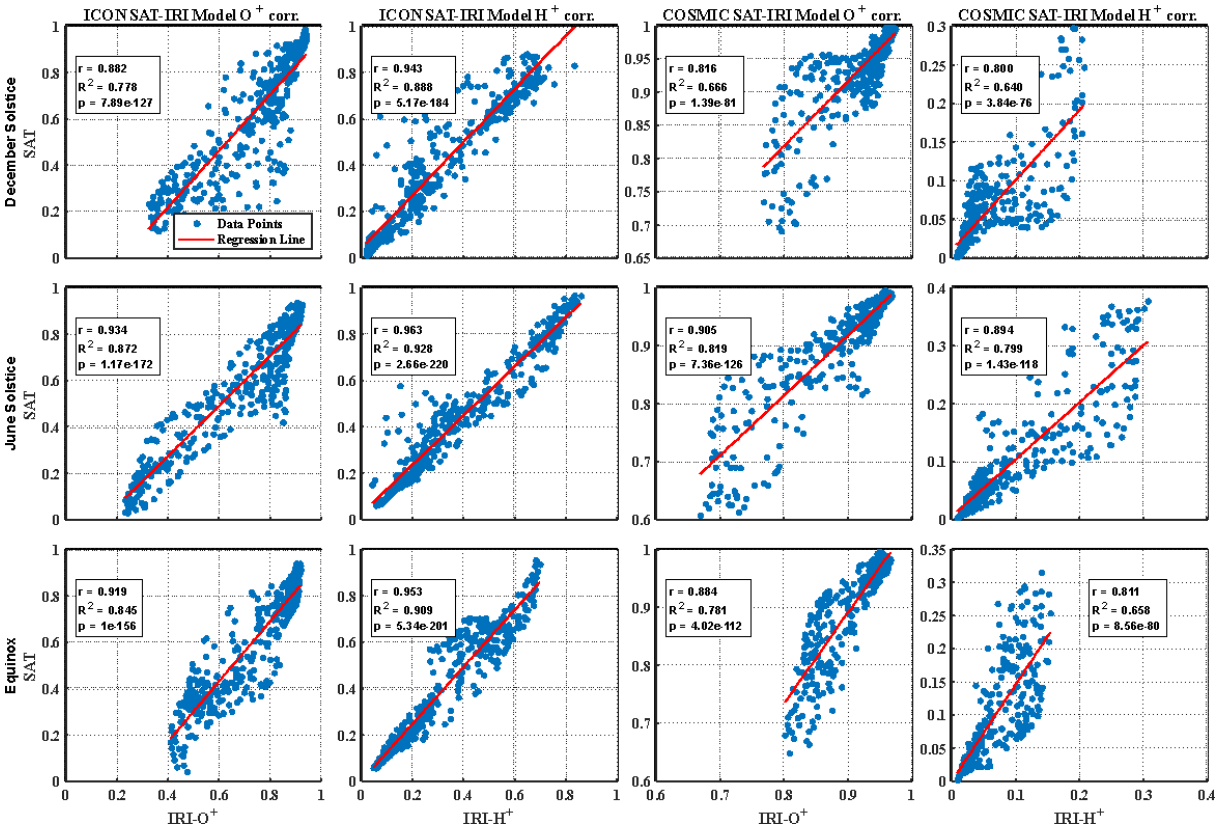

Figure 9. Seasonal correlation between both ICON and COSMIC-2 observations with their respective IRI-2020 model outputs for O^+ and H^+.

Off the equator, the r values increase significantly in all the seasons. During the June solstice, the correlations are higher and stable, generally above 0.9, for both ion fractions.

Figure 9 shows seasonal scatter plots comparing satellite-derived and IRI-2020 modeled topside ion fractions. The left panels correspond to ICON vs. IRI-2020 comparisons, while the right panels show COSMIC-2 vs. IRI-2020 comparisons. Each panel includes the linear Pearson correlation coefficient (r), coefficient of determination (R^2), and p-value.

For H^+ fractions, ICON measurement shows very strong agreement with IRI-2020 across all seasons, with r values exceeding ~0.90 and high R^2. The tight clustering along the regression line indicates that IRI-2020 reproduces the large-scale climatological variability of H^+ observed by ICON. COSMIC-2 exhibits similarly strong correlations for H^+, with increased scatter especially during solstice periods.

For O^+ fractions, correlations remain high but are systematically lower than for H^+. ICON vs. IRI-2020 O^+ comparisons show increased spread around the regression line, particularly during equinox, indicating larger deviations between modeled and observed O^+ fractions. COSMIC-2 vs. IRI-2020 O^+ correlations are comparable but display slightly tighter clustering during equinox than solstices. For both satellites, the highest correlations occur during June solstice ($r > \sim 0.9$). There is a large-scale agreement between the observations and model predictions, with all correlations statistically significant ($p \ll 0.01$).

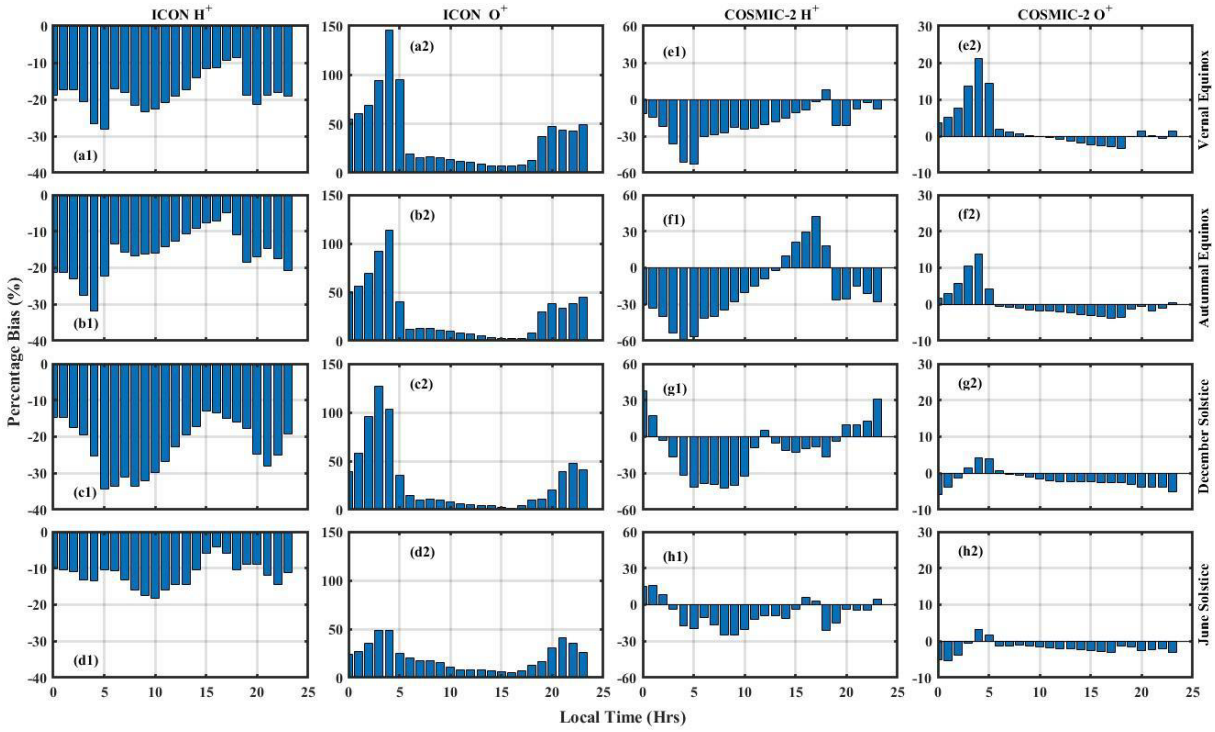

Figure 10. Seasonal median percentage bias of IRI-2020 relative to ICON and COSMIC-2 topside ion composition observations for H^+ and O^+ fractions. Positive (negative) values indicate IRI-2020 overestimation (underestimation). Panels show the biases in 1h bins as a function of local time for the vernal equinox, autumnal equinox, December solstice, and June solstice.

Figure 10 shows the seasonal percentage bias of IRI-2020 relative to ICON and COSMIC-2 topside H^+ and O^+ ion fraction observations. The percentage bias was computed as $(IRI_{fraction} - Satellite_{fraction})/(Satellite_{fraction} \times 100\%)$ at each grid point, excluding bins where satellite H^+ fractions were below 10^{-3}, avoiding numerical instability. Median bias values were used to provide estimate of seasonal systematic deviation. Figure 10 reveals that the seasonal biases are not uniform in local time. For H^+, (panels a1-d1, e1-h1), the strongest negative biases typically occur during dawn and dusk hours, particularly during equinoxes and December solstice. For O^+, ICON biases exhibit pronounced LT modulation (panels a2-d2), while COSMIC-2 biases remain weak and relatively flat across LT in all seasons (panels e2-h2).

Table 1 complements Fig. 10 and it shows the numerical summary of the seasonal median percentage bias for the ion fractions, separately for the vernal equinox, autumnal equinox, December solstice, and June solstice.

For H^+ fractions, IRI-2020 exhibits a systematic negative bias relative to both ICON and COSMIC-2 across all seasons, indicating a persistent underestimation of H^+ by the model. Against ICON, median biases range from approximately −11% to −22%, with the largest underestimation occurring during the December solstice. COSMIC-2 shows a similar but slightly higher magnitude, with median biases between −9% and −27%, and the highest underestimation occurring during the autumnal equinox.

For O^+ fractions, the bias behavior differs substantially between the two satellites. Relative to ICON, IRI-2020 shows a predominantly positive bias in all seasons, with median values between ~10% and ~18%, that is, systematically overestimating O^+ fractions. In contrast, COSMIC-2 O^+ shows substantially better agreement with the model. The biases are generally $\leq \pm 10\%$ and median values generally within ±2%.

Table 1. Median seasonal percentage bias of IRI-2020 relative to ICON and COSMIC-2 topside ion fraction observations. Positive (negative) values indicate IRI overestimation (underestimation).

Satellite	Ion fraction	Vernal Eq.	Autumnal Eq.	Dec Solstice	June Solstice
ICON	H^+ (Median Bias)	−18.86	−16.02	−21.18	−11.07
	O^+ (Median Bias)	17.76	12.76	10.77	17.30
COSMIC-2	H^+ (Median Bias)	−20.80	−26.21	−9.78	−9.13
	O^+ (Median Bias)	0.06	−1.27	−2.23	−2.05

4. Discussion

The results presented in Section 3 demonstrate that both ICON and COSMIC-2 satellites capture the major diurnal, seasonal, latitudinal, and longitudinal variations in the topside F-region O^+ and H^+ fractional compositions. While IRI-2020 reproduces the large-scale diurnal and seasonal behavior of ion composition, some systematic differences remain.

4.1 Seasonal control of topside ion fractions

Considering ICON and COSMIC-2 observations (Figs. 1, 2, 5, and 6), the seasonal behavior of H^+ and O^+ fractions is driven by thermosphere-ionosphere coupling and solar EUV radiation. Daytime O^+ dominance reflects solar EUV ionization and confinement by low-latitude electrodynamics, while nighttime H^+ enhancement arises from reduced photoionization, chemical recombination of O^+, and downward diffusion of lighter ions from the plasmasphere. Torr, et al., (1979) noted that the plasma distribution process begins with the ionization of atomic oxygen in the F region, which originates from the photo-dissociation of molecular oxygen in the lower thermosphere. The upper atmosphere is a highly complex system, primarily controlled by variable solar EUV and UV radiation together with dynamical processes. As a result, the daytime ionosphere in the F2 region is dominated by O^+ ions. At night, the absence of solar radiation and ongoing chemical loss processes in the F2 region led to a reduction in O^+ density (González et al., 1992; Kutiev et al., 1980). Consequently, the relative distributions of O^+ and H^+ ions are strongly influenced by solar radiation conditions (Choi et al., 2022).

Seasonal differences in topside ion composition are mainly controlled by changes in solar illumination and the large-scale thermospheric circulation. During solstice conditions, the summer hemisphere receives more solar radiation, which generally leads to higher temperatures and larger scale heights. Under these conditions, O^+ tends to remain dominant to higher altitudes. In contrast, during winter conditions, reduced solar illumination and lower neutral oxygen densities favor a relative increase in lighter ions, such as H^+, in the topside ionosphere.

IRI-2020 reproduces the overall seasonal behavior and hemispheric differences, with higher O^+ fractions in the summer hemisphere and higher H^+ fractions in the winter hemisphere. However, the model systematically underestimates the strength of the observed seasonal contrast, particularly for O^+. Part of the discrepancy may reflect the presence of other ion species, such as He^+ and N^+, which are included in the IRI ion composition model formulation and can influence the relative O^+ and H^+ fractions compared to the ICON and COSMIC-2 satellite data which is based on the RPA method and is unable to distinguish between O^+ and N^+ and has limited ability to detect He^+ due to its low abundance in most conditions.

4.2 Local-time effects

O^+ peaks during the day while H^+ peaks during the night (Figs. 1, 3, 5, and 7). During daytime, solar extreme ultraviolet (EUV) radiation plays a dominant role in generating F2-region ionospheric plasma through photoionization, producing ion-electron pairs. Plasma density increases after sunrise and typically peaks around 12:00-14:00 LT. After noon, the increasing solar zenith angle reduces ion production, leading to a gradual decline in plasma density. As a result, ionospheric plasma exhibits a pronounced diurnal variation (Choi et al., 2022). Furthermore, equatorial $\mathbf{E} \times \mathbf{B}$ drifts lift F-region plasma, dominated by O^+ ions, to higher altitudes. The uplifted plasma then diffuses along magnetic field lines under the influence of gravity and pressure gradients, producing two ionization crests on either side of the equator and a depletion region directly over the geomagnetic equator (Anderson et al., 2004; Kil et al., 2007; Ram et al., 2010; Schunk and Nagy, 1978). The strongest model-data deviations occur near pre-dawn and after dusk (Figs. 3 and 7), when rapid transitions in photoionization and vertical plasma transport dominate. These processes evolve on short timescales and generate sharp gradients in the O^+/H^+ transition height (Pignalberi et al., 2025; Ram et al., 2010; Vaishnav et al., 2021). ICON/COSMIC-2 resolve these transitions clearly, while IRI-2020 smooths them due to its formulation.

ICON observed H^+ consistently shows better agreement with IRI-2020 than O^+ (Figs. 3, 4 and 9). The reason can be that RPA has difficulties distinguishing between H^+ and He^+ because of low solar activity and thus a relatively low He^+ fraction.

Prereversal enhancement (PRE)-driven composition changes can help to explain the observed dusk biases and evening discrepancies between satellite observations and model predictions (Figs. 3 and 7). PRE introduces strong dusk-sector variability in O^+ and H^+ fractions that is difficult for IRI-2020 to predict. ICON measurements seem to detect sharper LT gradients in H^+ fraction because it samples closer to the O^+/H^+ transition height (Fig. 3) while COSMIC-2 captures a gradual post-PRE increase in H^+ fraction (Fig. 7). Seasonally, previous studies have shown that the evening PRE varies with both season and solar activity (Fejer et al., 1981, 1991, 2008; Kil et al., 2007, 2009). The amplitude of the PRE-related vertical plasma drift generally increases with increasing solar flux (Fejer, 1999; Fejer et al., 1991; Kil et al., 2011). In addition, PRE exhibits a clear seasonal dependence, with the strongest enhancements typically occurring during the equinoxes (Figs. 3 and 7, panels a1, b1, e1 and f1) and the weakest during the June solstice (Figs. 3 and 7, panels c1, d1, g1 and h1) (Fesen et al., 2000).

4.3 Latitude and longitude variations

Latitudinal structures of ion fractions reflect the balance between production, loss and transport (Su et al., 2005; Třísková et al., 1998). At low latitudes and especially near the magnetic equator, vertical $E \times B$ drift together with production and transport uplifts O^+ to higher altitudes, giving rise to the latitudinal gradients in O^+ density observed by the satellites (Figs. 1, 4, and 5). IRI-2020 reproduces the large-scale pattern but underestimates peak gradients due to its smoothing effects given by limited resolution.

Complex longitudinal variability seen in ICON observations (Fig. 2) and during equinoxes in COSMIC-2 (Fig. 6) can be a reflection of modulation by non-migrating tides and thermospheric winds (e.g., Pedatella et al., 2011). These lower-atmosphere-driven processes could influence the composition of the ion fractions that is largely absent in IRI-2020. The weak longitudinal predictions by the model, could arise from the fact that the TBT15 option in IRI-2020 model does not explicitly include variation with longitude in its formulation (Truhlik et al., 2015).

4.4 ICON versus COSMIC-2 agreement with IRI-2020

The statistical comparison of solar flux index ($F_{10.7}$)) of the data during ICON and COSMIC-2 (Table 2) could explain why COSMIC-2 observations tend to give a better agreement with IRI-2020 than ICON. COSMIC-2 period (2022-2023) corresponds to higher solar flux levels than the ICON period (2020-2021). COSMIC-2 samples ionosphere during higher solar activity, with larger mean and median F10.7 values. In contrast, ICON measurements are dominated by lower solar flux conditions.

Table 2. Statistical summary of the $\boldsymbol{F_{10.7}}$ (sfu) during the ICON and COSMIC-2 observation periods, reflecting the different solar activity environments encountered by each mission.

Statistics Metrics	ICON	COSMIC
Mean	92.62	123.33
Median	82.60	131.60
Standard Deviation	22.86	33.15
Lower quartile	73.1	87.95
Upper quartile	118.17	151.03

Table 2 shows that COSMIC-2 has higher values across all metrics (Mean $\boldsymbol{F_{10.7}}$: 123.33, Median: 131.60) compared to ICON (Mean $\boldsymbol{F_{10.7}}$: 92.62, Median: 82.60). The low solar activity during these observations plays a critical role. The TBT15 model within IRI-2020 tends to be more reliable during high solar activity since it relies on much larger dataset during high solar activity than during low solar activity. Also, as mentioned RPA has difficulties distinguishing between H^+ and He^+ because of low solar activity and thus ICON ion composition might show larger H^+ fraction.

Another possible source of differences can be due to differences in altitude because COSMIC-2 orbits lower and (in combination with higher solar activity) measures generally below the O^+/H^+ transition region as can be estimated from Fig. 7, since O^+ fraction is much higher than H^+ fraction. In contrast, ICON samples at a higher altitude (~580 km), closer to the transition region as it is during low solar activity and as can be seen in Fig. 3, where the concentrations of O^+ and H^+ alternate depending on the local time. At this level, small changes in the environment may cause sharp changes in (Harding et al., 2025; Wu et al., 2025). This can further explain why ICON's values differ from IRI-2020 but its biases with IRI-2020 are more structured. It is measuring a highly dynamic transition zone that climatological models struggle to replicate (Bilitza et al., 2022; Gao et al., 2024; Koehnlein, 1989; Vaishnav et al., 2021).

5. Conclusions

This study presents detailed climatological evaluation of the IRI-2020 model (latest version) in reproducing low-latitude topside ion composition using complementary in situ observations from the ICON and COSMIC-2 satellite missions. By exploiting the distinct solar activity and altitude sampling characteristics of these two datasets, the analysis provides new diagnostic insight that is not accessible through single-mission evaluations.

The results demonstrate that IRI-2020 reliably reproduces the large-scale climatological structure of topside ion composition, including the dominant daytime O^+ and nighttime H^+ regimes and their broad seasonal variability. However, systematic biases seem persist near the O^+/H^+ transition region. ICON-based comparisons reveal consistent overestimation of O^+ and underestimation of H^+, suggesting that the modeled transition height may be, on average, positioned too high under climatological conditions of low solar activity. In contrast, COSMIC-2-based comparisons show substantially smaller biases at medium solar activity.

Furthermore, our result shows that the IRI-2020 model-data discrepancies are strongly modulated by local time, with the largest differences occurring near dawn and dusk when rapid electrodynamic, transport and photochemical processes dominate ionospheric restructuring. These findings point out to the limitations of monthly-mean empirical models with limited temporal variation (given by spherical harmonics up to 6^{th} order in the TBT15 model) in representing sharp local-time transitions.

In summary, this study work provides the scientific community with new information by providing interpreted assessment of the ion composition IRI-2020 model performance in the low-latitude topside ionosphere. The results emphasize the importance of detailed model evaluation and demonstrate the value of combining complementary satellite datasets to diagnose model limitations. Future improvements to empirical ionospheric models should benefit from better representation of temporal and spatial resolution, and better description of variation of ion composition with geophysical parameters.

Data availability statement. Data can be downloaded at: https://data.cosmic.ucar.edu. and https://spdf.gsfc.nasa.gov.

Acknowledgements. The authors acknowledge that this research was initiated during the International Reference Ionosphere (IRI) 2024-A COSPAR Capacity-Building Workshop Training Week, held from 2-6 September 2024 in Kilifi, Kenya. The workshop provided an excellent platform for scientific exchange and mentorship, which contributed to the formulation of the research concept and the commencement of this work.
We gratefully acknowledge the availability of COSMIC-2 (Constellation Observing System for Meteorology, Ionosphere, and Climate-2) satellite data provided by the University Corporation for Atmospheric Research (UCAR) COSMIC Data Analysis and Archive Center (CDAAC), accessible at https://data.cosmic.ucar.edu. We also acknowledge the use of ICON (Ionospheric Connection Explorer) satellite data obtained through the NASA Space Physics Data Facility (SPDF), available at https://spdf.gsfc.nasa.gov.

References

Anderson, D., A. Anghel, J. Chau and O. Veliz (2004). Daytime vertical E × B drift velocities inferred from ground-based magnetometer observations at low latitudes, Space Weather, 2, 11, 1-9, doi:10.1029/2004sw000095.

Anthes, R. and W. Schreiner (2019). Six new satellites watch the atmosphere over Earth's equator, Eos, 100, doi:10.1029/2019EO131779.

Bilitza, D., D. Altadill, V. Truhlik, V. Shubin et al. (2017). International Reference Ionosphere 2016: From ionospheric climate to real-time weather predictions, Space Weather, 15(2), 418-429, doi:10.1002/2016SW001593.

Bilitza, D., M. Pezzopane, V. Truhlik, D. Altadill et al. (2022). The International Reference Ionosphere Model: A Review and Description of an Ionospheric Benchmark, Rev. Geophys, 60, 4, doi:10.1029/2022RG000792.

Cherniak, I., I. Zakharenkova, J. Braun, Q. Wu et al. (2021). Accuracy assessment of the quiet-time ionospheric F2 peak parameters as derived from COSMIC-2 multi-GNSS radio occultation measurements. J. Space Weather Space Clim., 11, 1-14, doi:10.1051/swsc/2020080.

Choi, J., C. Lin, S. Chen and J. Lin (2022). Validation of in-situ ionospheric density using FORMOSAT-7/COSMIC-2 IVM and ICON IVM, 1-20.

Danilov, A. D. and A. P. Yaichnikov (1985). A new model of the ion composition at 75 to 1000 km for IRI. Adv. Space Res., 5, 7, 75-79, doi:10.1016/0273-1177(85)90360-6.

Fejer, B. G. (1999). Effects of the vertical plasma drift velocity on the generation and evolution of equatorial spread F. J. Geophys. Res.: Space Phys., 104, A9, 19859-19869, doi:10.1029/1999ja900271.

Fejer, B. G., E. R. De Paula, R. F. Woodman and S. A. Gonzales (1991). Extensive Incoherent Scatter Radar Observations, J. Geophys. Res., 96, June 1988, 13901-13906.

Fejer, B. G., D. T. Farley and C. A. Gonzales (1981). Drifts Show No Such Reversals, a Result Which Has, 86, 215-218.

Fejer, B. G., J. W. Jensen and S. Y. Su (2008). Quiet time equatorial F region vertical plasma drift model derived from ROCSAT-1 observations. J. Geophys. Res.: Space Phys., 113, 5, 1-10, doi:10.1029/2007JA012801.

Fesen, C. G., G. Crowley, R. G. Roble, A. D. Richmond and B. G. Fejer (2000). Simulation of the pre-reversal enhancement in the low latitude vertical ion drifts, Geophys Res Lett, 27, 13, 1851-1854.

Gao, S., C. Xiong, Z. Zhu, W. Zhan et al. (2024). Altitudinal Variation of O^+ Scale Height at the Equatorial Topside Ionosphere, J. Geophys. Res.: Space Physics, 129, 12, 1-17, doi:10.1029/2024JA033033.

González, S. A., B. G. Fejer, R. A. Heelis and W. B. Hanson (1992). Ion composition of the topside equatorial ionosphere during solar minimum, J. Geophys. Res.: Space Phys., 97, A4, 4299-4303, doi:10.1029/91ja03111.

Han, T., H. Le, S. R. Zhang, V. Truhlik et al. (2025). Evaluations of two ion temperature models in IRI-2020 based on the observations from ICON and COSMIC-2 IVM. Adv. Space Res., 75, 5, 4317-4326, doi:10.1016/j.asr.2024.06.025.

Harding, B. J., M. C. Serrano, L. C. Gasque, J. Wu et al. (2025). Wind-Driven Variability in the Prereversal Enhancement of the Equatorial Vertical Plasma Drift: Climatologies Observed by ICON, J. Geophys. Res.: Space Phys., 130, 1, doi:10.1029/2024JA033279.

Hazarika, A., K. Bhuyan, B. R. Kalita, P. K. Bhuyan and A. Borgohain (2024). Evaluation of the improvement of IRI 2020 over IRI 2016 around 100°E during low solar activity 3.2 Comparison between IRI 2016 and IRI 2020 simulations with GIM-TEC variation 3. Results and Discussion 3.1 Comparison between IRI 2016 and IRI 2020 simu, 2, 1, 22-25.

Heelis, R. A., R. A. Stoneback, M. D Perdue, M. D Depew et al. (2017). Ion Velocity Measurements for the Ionospheric Connections Explorer, Space Sci. Rev., 212, 1-2, 615-629, doi:10.1007/s11214-017-0383-3.

Immel, T. J., S. L. England, S. B. Mende, R. A. Heelis et al. (2018). The Ionospheric Connection Explorer Mission: Mission Goals and Design, Space Sci. Rev., 214, Springer Science+Business Media B.V., part of Springer Nature, doi:10.1007/s11214-017-0449-2.

Kil, H. and S. J. Oh (2011). Dependence of the evening prereversal enhancement of the vertical plasma drift on geophysical parameters, J. Geophys. Res.: Space Phys., 116, 5, 1-8, doi:10.1029/2010JA016352.

Kil, H., S. J. Oh, M. C. Kelley, L. J. Paxton et al. (2007). Longitudinal structure of the vertical E x B drift and ion density seen from ROCSAT-1, Geophys. Res. Lett., 34, 14, 3-7, doi:10.1029/2007GL030018.

Kil, H., L. J. Paxton and S. J. Oh (2009). Global bubble distribution seen from ROCSAT-1 and its association with the evening prereversal enhancement, J. Geophys. Res.: Space Phys., 114, 6, 1-9, doi:10.1029/2008JA013672.

Kotov, D. V., V. Truhlík, P. G. Richards, S. Stankov et al. (2015). Night-time light ion transition height behaviour over the Kharkiv (50°N, 36°E) IS radar during the equinoxes of 2006-2010, J. Atmos. Solar-Terrestrial Phys., 132, 1-12, doi:10.1016/j.jastp.2015.06.004.

Köhnlein, W. (1989). A model of the terrestrial ionosphere in the altitude interval 50-4000 km i. atomic ions (H^+, He^+, N^+, O^+)*. Deutsche Forschungsanstalt Fzir Luft-Und Raumfahrt (DLR), 8031 Wessling, and Astronomical Institutes, University of Bonn, 5300 F. R. Germany, 53-100.

Kutiev, I., R. A. Heelis and S. Sanatani (1980). The behavior of the O^+-H^+ transition level at solar maximum, J. Geophys. Res.: Space Phys., 85, A5, 2366-2372, doi:10.1029/ja085ia05p02366.

Lühr, H. and C. Xiong (2010). IRI-2007 model overestimates electron density during the 23/24 solar minimum. Geophys. Res. Lett., 37, 23, 1-5, doi:10.1029/2010GL045430.

Mainul, M. and N. Jakowski (2012). Ionospheric Propagation Effects on GNSS Signals and New Correction Approaches. Global Navigation Satellite Systems: Signal, Theory and Applications, February, doi:10.5772/30090.

Pignalberi, A., D. Bilitza, P. Coïsson, H. Haralambous et al. (2025). Validation of the IRI-2020 topside ionosphere options through in-situ electron density observations by low-Earth-orbit satellites, Adv. Space Res., 75, 5, 4192-4216, doi:10.1016/j.asr.2024.05.056.

Ram, T. S., C. H. Liu, S. Y. Su and R. A. Heelis (2010). A comparison of ionospheric O^+/light-ion transition height derived from ion-composition measurements and the topside ion density profiles over equatorial latitudes, Geophys. Res. Lett., 37, 20, doi:10.1029/2010GL045199.

Schunk, R. W. and A. F. Nagy (1978). Electron temperatures in the F region of the ionosphere: Theory and observations, Rev. Geophys, 16, 3, 355-399, doi:10.1029/RG016i003p00355.

Su, S. Y., C. K. Chao, H. C. Yeh and R. A. Heelis (2005). Seasonal and latitudinal distributions of the dominant light ions at 600 km topside ionosphere from 1999 to 2002, J. Geophys. Res.: Space Physics, 110, A1, 1-15, doi:10.1029/2004JA010564.

Torr, M. R., D. G. Torr, R. A. Ong and H. E. Hinteregger (1979). Ionization frequencies for major thermaspheric, Geophys. Res. Lett., 6, 10, 771-774.

Třísková, L., V. Truhlík, J. Šmilauer and Y. A Shultchishin (1998). Comparison of O^+/H^+ and $O^+/(H^+ + He^+)$ transition levels, Adv. Space Res., 22, 6, 895-898, doi:10.1016/S0273-1177(98)00119-7.

Třísková, L., V. Truhlík and J. Šmilauer (2003). An empirical model of ion composition in the outer ionosphere, Adv. Space Res., 31, 3, 653-663, doi:10.1016/S0273-1177(03)00040-1.

Truhlik, V., D. Bilitza and L. Triskova (2015). Towards better description of solar activity variation in the International Reference Ionosphere topside ion composition model, Adv. Space Res., 55, 8, 2099-2105. doi:10.1016/j.asr.2014.07.033.

Vaishnav, R., Y. Jin, M. G. Mostafa, S. R. Aziz et al. (2021). Study of the upper transition height using ISR observations and IRI predictions over Arecibo, Adv. Space Res., 68, 5, 2177-2185, doi:10.1016/j.asr.2020.10.010.

Wu, J. W., C. Xiong, Y. Y. Huang and Y. L. Zhou (2025). Vertical gradients of neutral winds observed by ICON and estimated by the Horizontal Wind Model during the geomagnetic storm on August 26-28, 2021, Earth Planet. Phys., 9, 1, 69-80, doi:10.26464/epp2024033.

***CORRESPONDING AUTHOR: Awuor ADERO**,
Technical University of Kenya, Department of Physics, Earth and Environmental Sciences, Nairobi, Kenya
e-mail: awuor.adero@tukenya.ac.ke